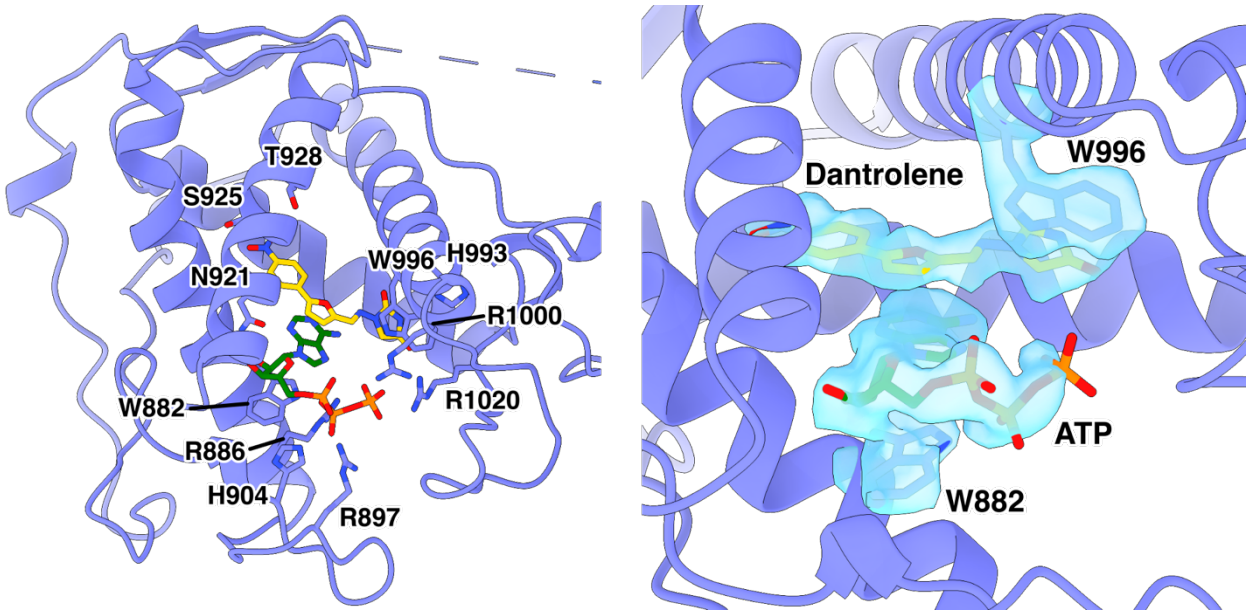

Figure S1: ATP binds in RY12 with dantrolene. The atomic model of RY12 is colored in light purple. Like Dan/ADP, dantrolene and ATP are flanked by W996 and W882.

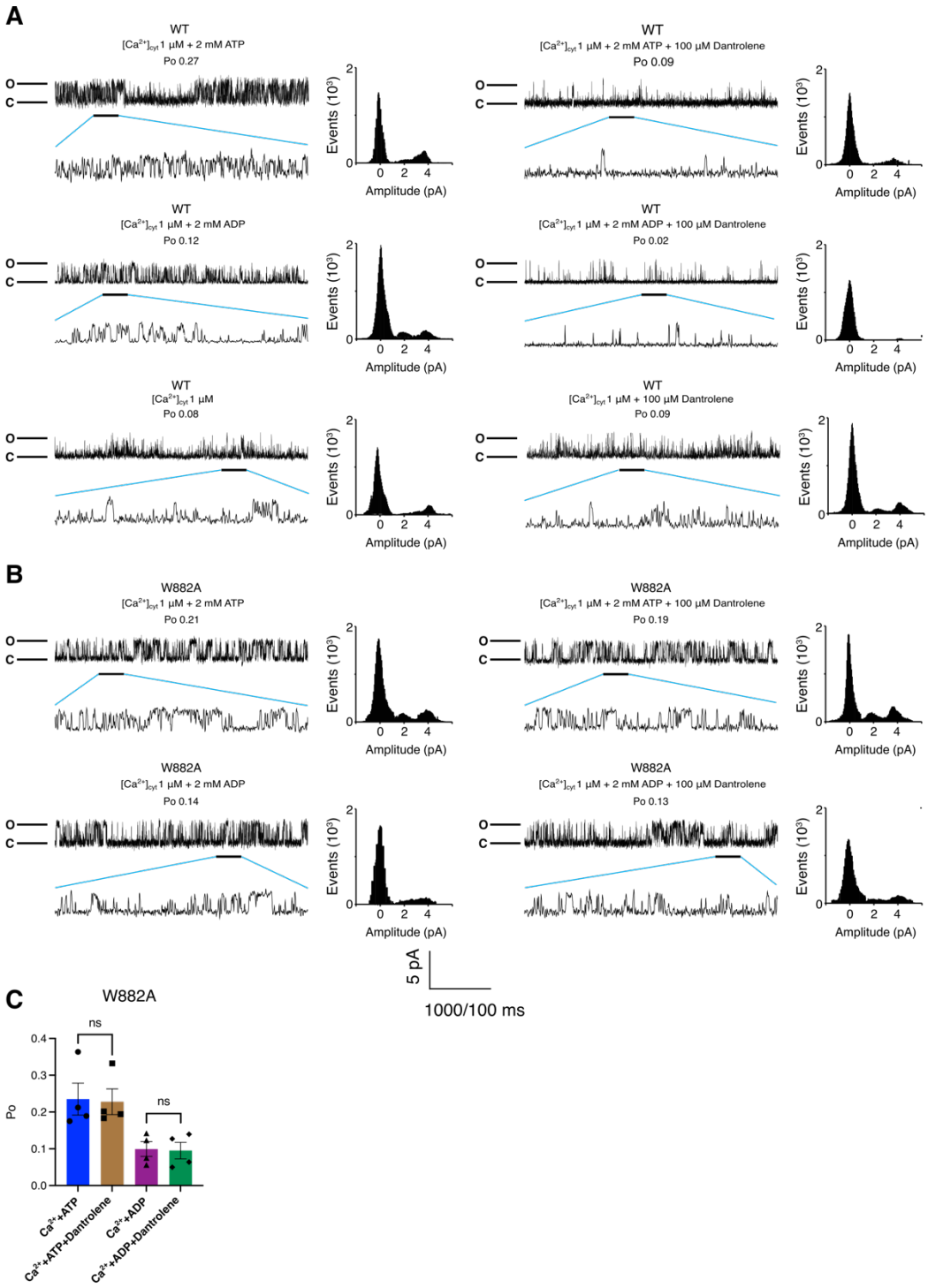

Figure S2: The current traces of wild-type & W882A mutant RyR1
A. Single-channel traces of wild-type (WT) RyR1 in a planar lipid bilayer after the addition of 1 μM Ca^{2+} with 2 mM ATP, 1 μM Ca^{2+} with 2 mM ADP, and 1 μM Ca^{2+} alone. Amplitude histograms for each condition are shown by the current traces. The agonist effect of each ligand is abolished by the addition of 100 μM dantrolene.

B. Single-channel traces of W882A mutant RyR1 in a planar lipid bilayer after the addition of 1 μM Ca^{2+} with 2 mM ATP and 1 μM Ca^{2+} with 2 mM ADP. Amplitude histograms for each condition are shown by the current traces. The agonist effects of ATP and ADP on W882A RyR1 are not abolished by the addition of 100 μM dantrolene. **C.** Quantification of single channel lipid bilayer recordings on W882A mutant RyR1 microsome in response to 100 μM dantrolene. 2 mM ATP or ADP was first added before addition of dantrolene (n=4, data point presented as mean ± SD). The *cis* [Ca^{2+}], representing the cytoplasmic compartment, was kept at 1 μM for all conditions.

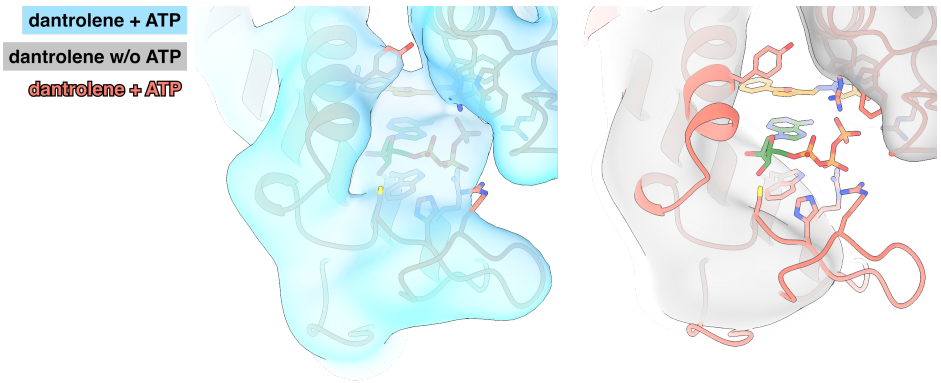

Figure S3: Without ATP, Dantrolene does not bind in RY12 (Dantrolene/Mg^{2+}). Lowpass-filtered cryoEM maps from Dan/ATP/4CmC/Caffeine/Mg^{2+} (skyblue) and Dan/Mg^{2+} (grey) datasets. The RY12 domain structure complexed with dantrolene, and ATP is colored in salmon.

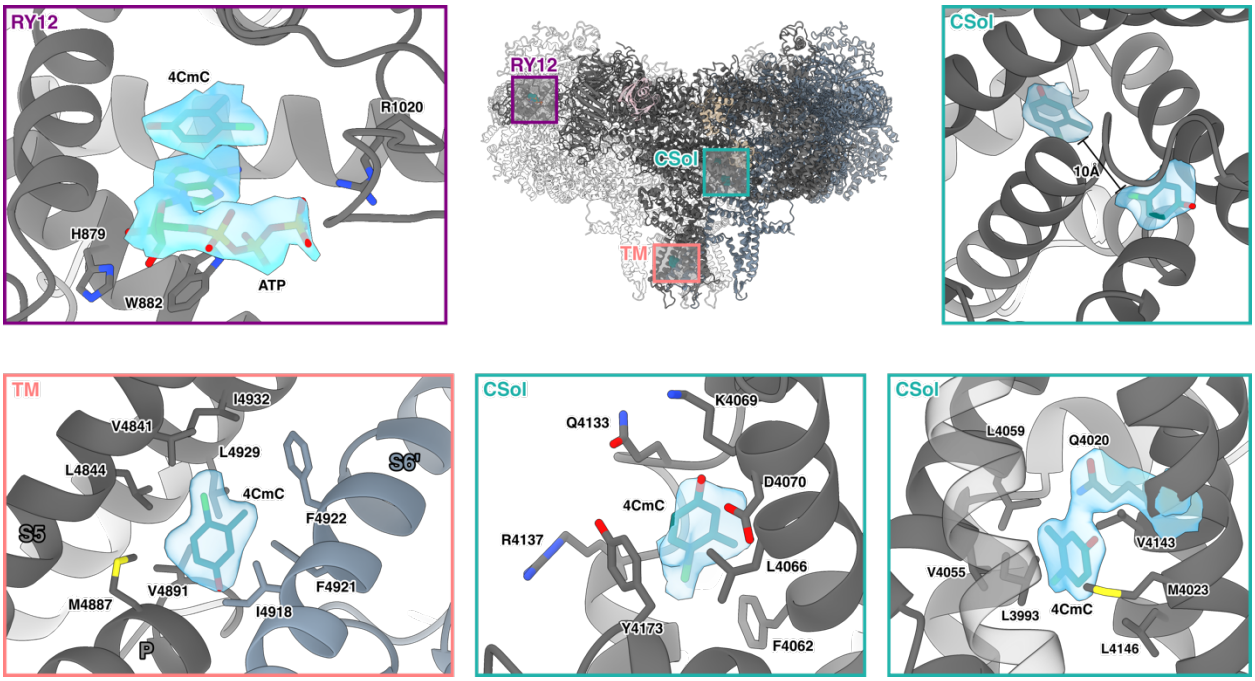

Figure S4: Different 4CmC binding sites on RyR1. 4CmC and ATP bind together in RY12 (purple box). The two 4CmC binding sites in CSol are ~10Å apart from each other (teal box). 4CmC also can dock in between P and S6 helices in TM (salmon box).

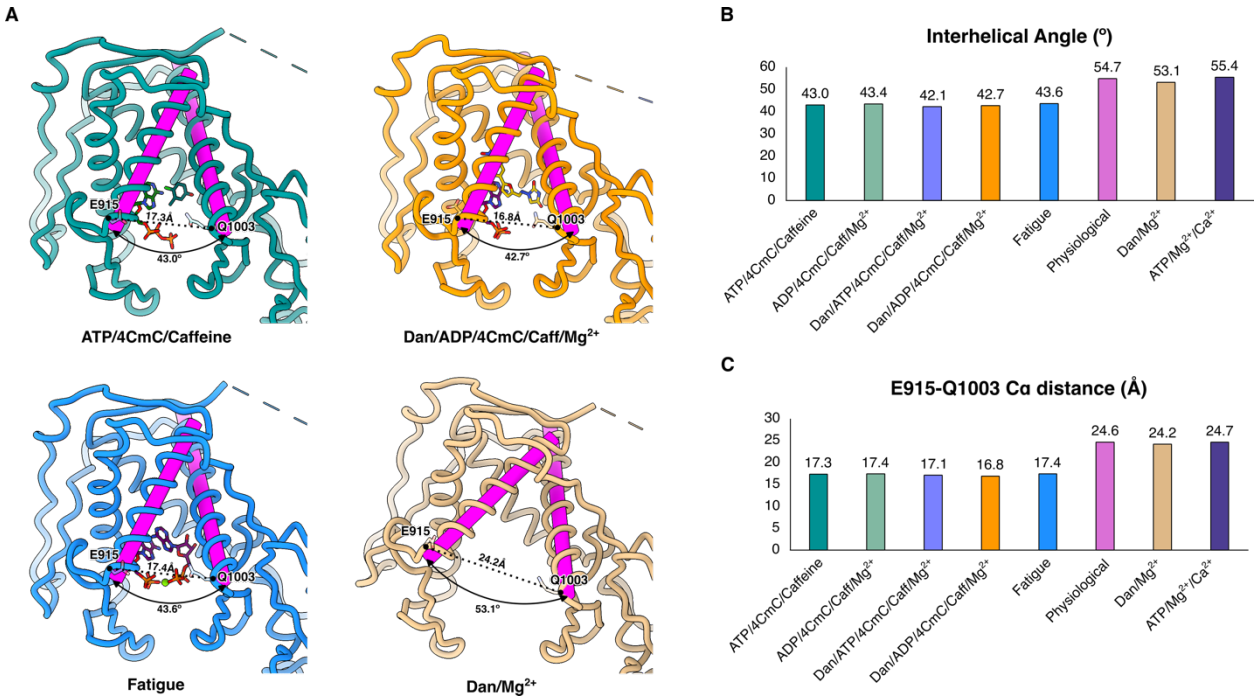

Figure S5: Changes in interhelical angles and Cα distance between E915 and Q1003 in RY12 upon conformational changes.

A. The magenta cylinder objects were generated in *ChimeraX* for the two α-helices (E915-A934 and P979-A1002) forming the RY12 clamp. The interhelical angles were calculated by measuring the rotational angles between the two cylinders for each dataset. The outermost subdomain of RY12 closes as the ligands bind in the RY12 binding cleft.

B. Quantification of the interhelical angle measurements. There is ~11.4° change of the interhelical angles between the apo and the holo states.

C. Quantification of the E915-Q1003 Cα distance measurements. There is ~7.3 Å difference between the apo and the holo states.

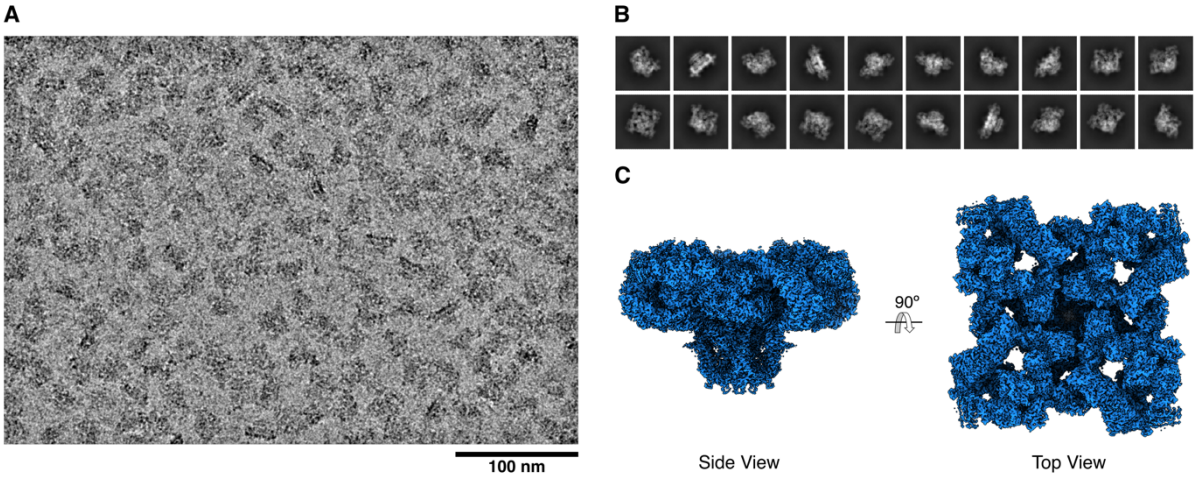

Figure S6: (**A**) A representative cryoEM micrograph of the Fatigue dataset (5,405 micrographs), (**B**) Representative 2D class averages, and (**C**) a combined 3D map was prepared by combining density-modified local maps (Fatigue).

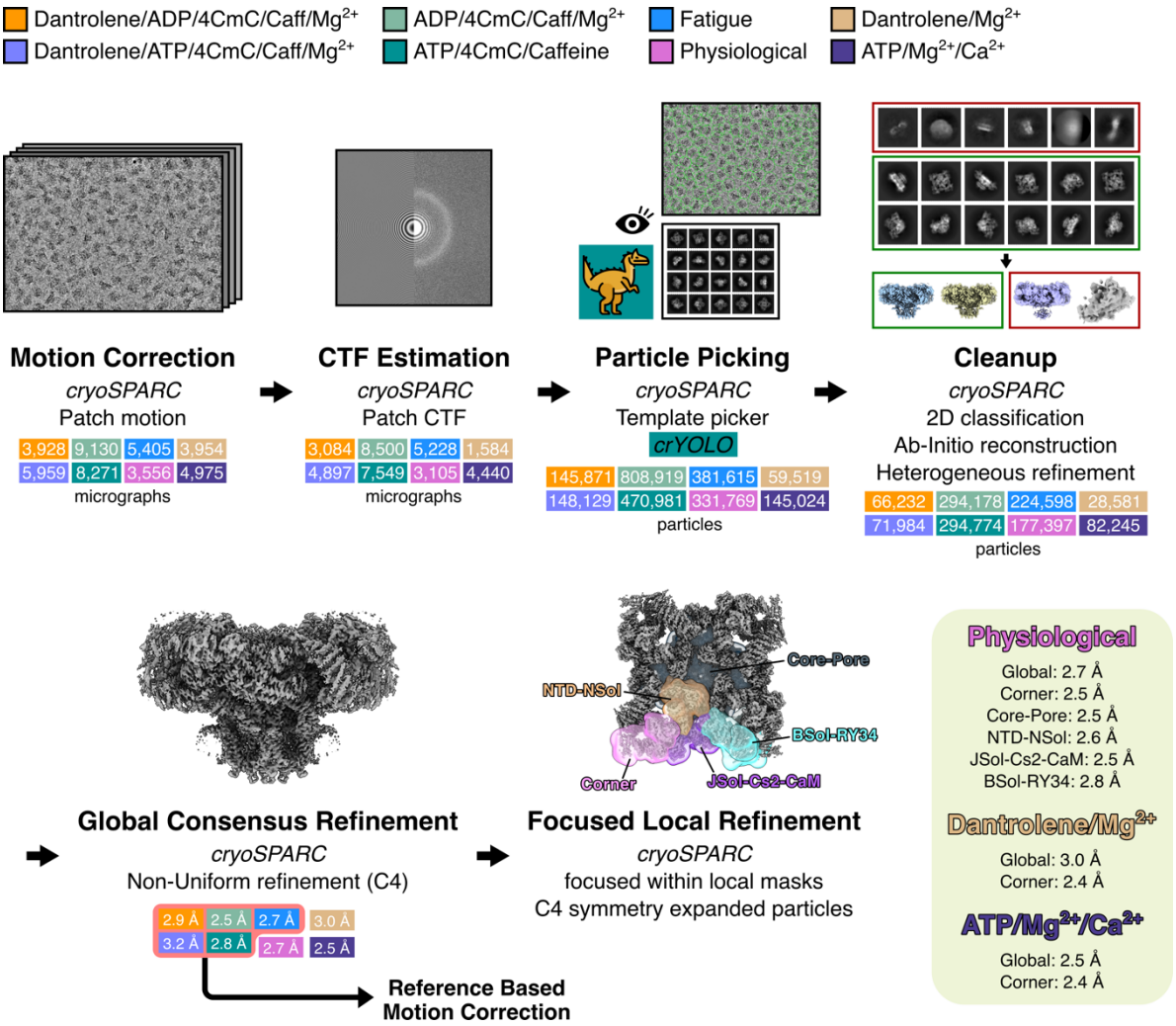

Figure S7: The general cryoEM processing workflow.
A flow chart of the generalized cryoEM image processing for the eight color-coded datasets. Particles were picked using *crYOLO* for the ATP/4CmC/Caffeine dataset. Out of the eight datasets, Dan/ADP/4CmC/Caff/Mg^{2+}, Dan/ATP/4CmC/Caff/Mg^{2+}, ADP/4CmC/Caff/Mg^{2+}, ATP/4CmC/Caff, & Fatigue datasets were subjected to reference-based motion correction in *cryoSPARC*.

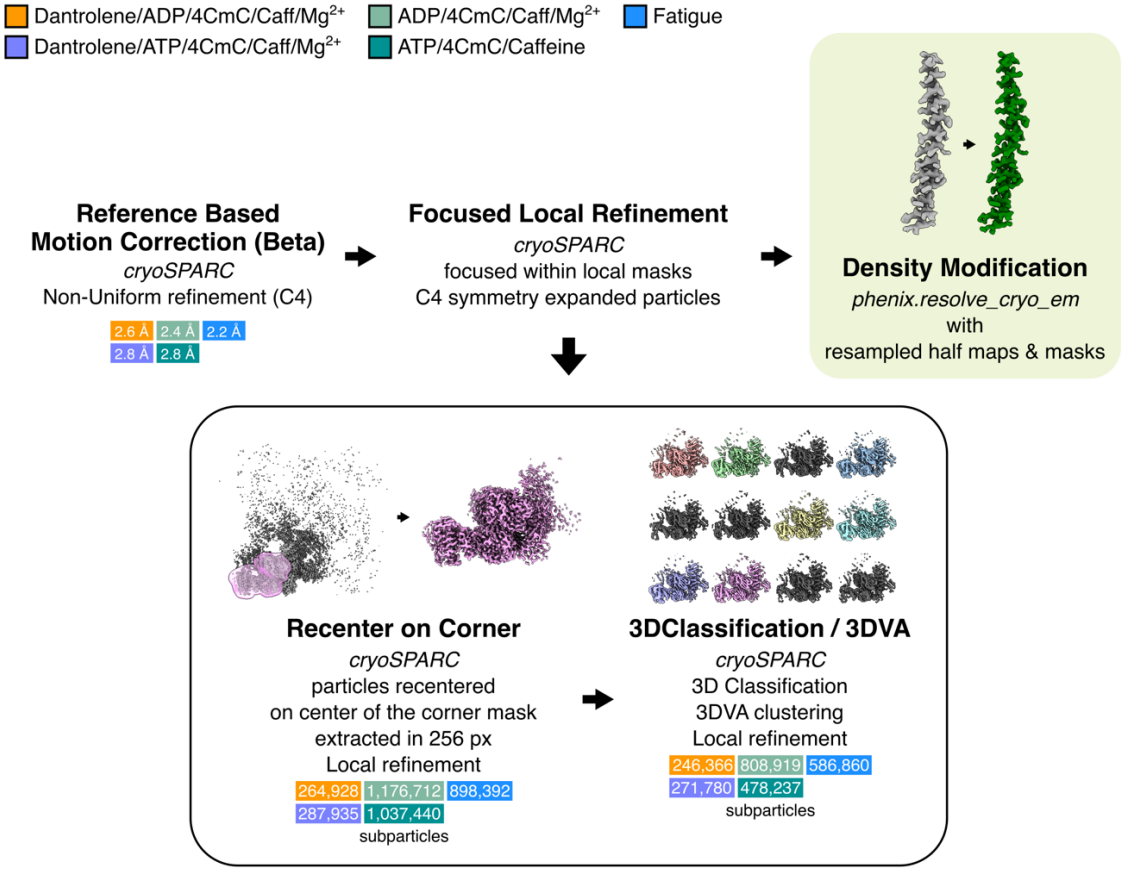

Figure S8: Flowchart of cryoEM image processing for the five datasets (Dan/ADP/4CmC/Caff/Mg^{2+}; orange, Dan/ATP/4CmC/Caff/Mg^{2+}; orchid, ADP/4CmC/Caff/Mg^{2+}; light green, ATP/4CmC/Caff; teal, & Fatigue; blue) that were subjected to Reference-based motion correction, recentering on corner masks and subparticle extraction, 3D Variability Analysis (3DVA) clustering, and 3D classification of the subparticles in *cryoSPARC*. The focused local refinement and density modification steps for the regions other than the corner region were kept the same for all eight datasets.

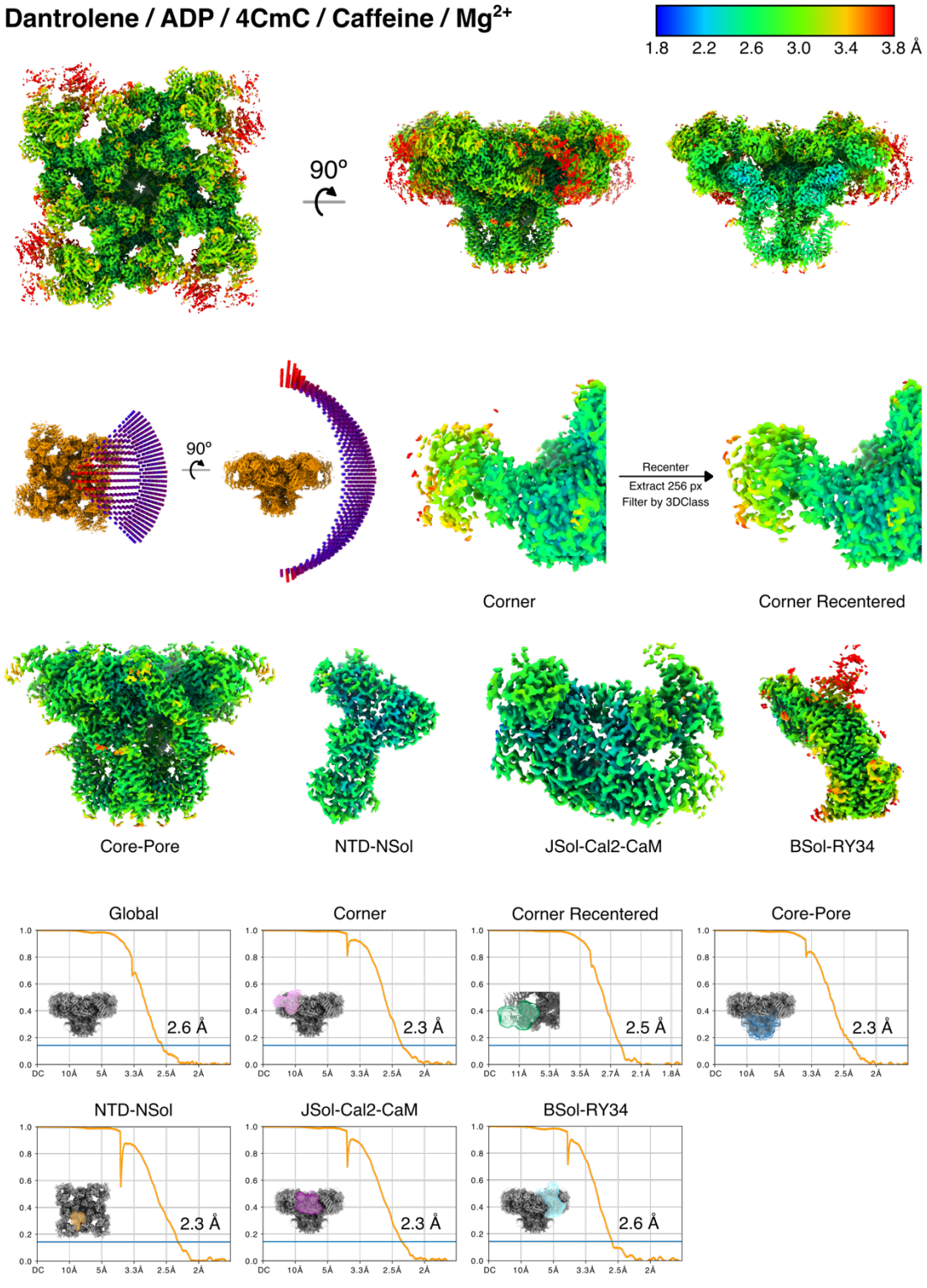

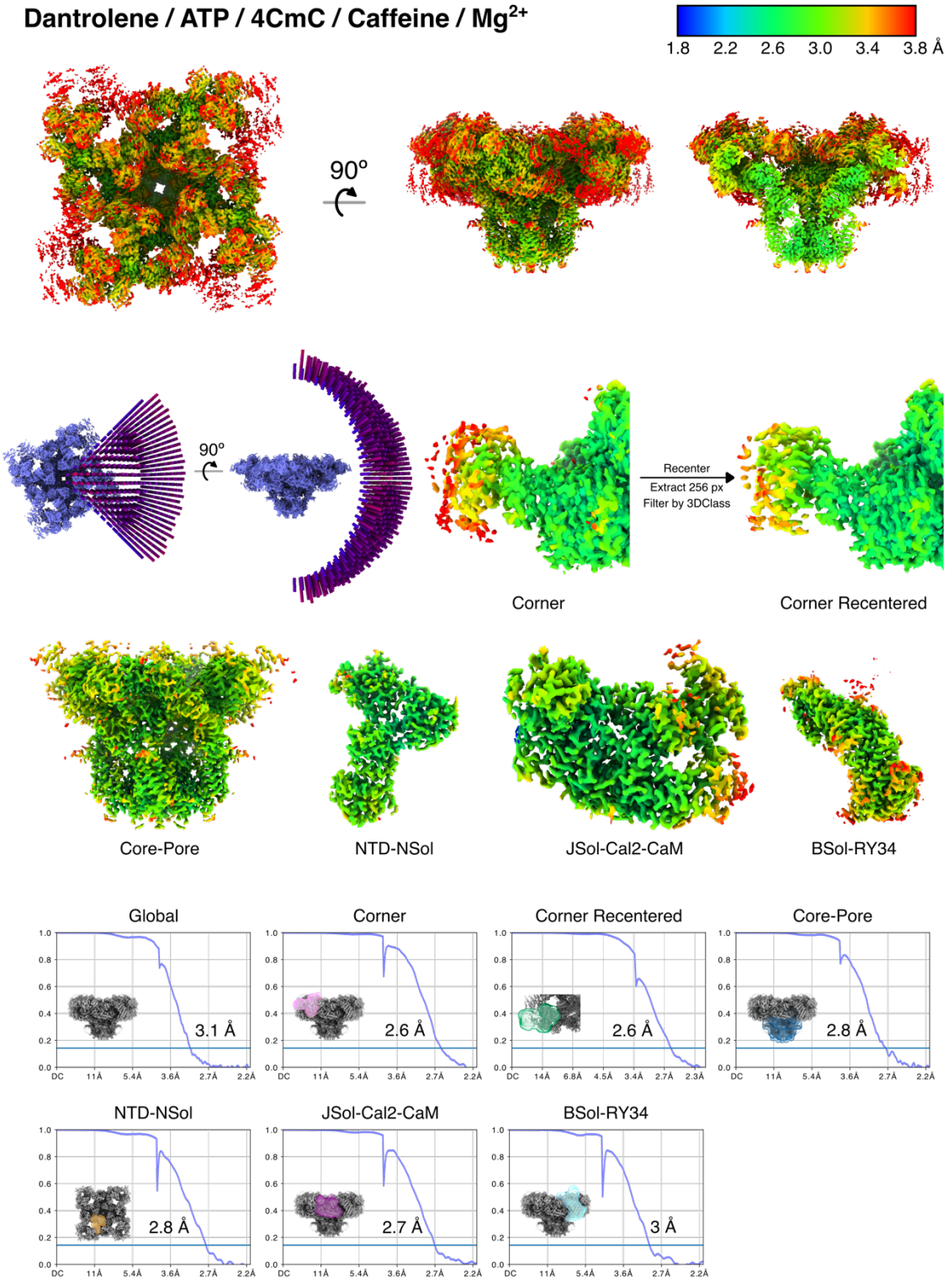

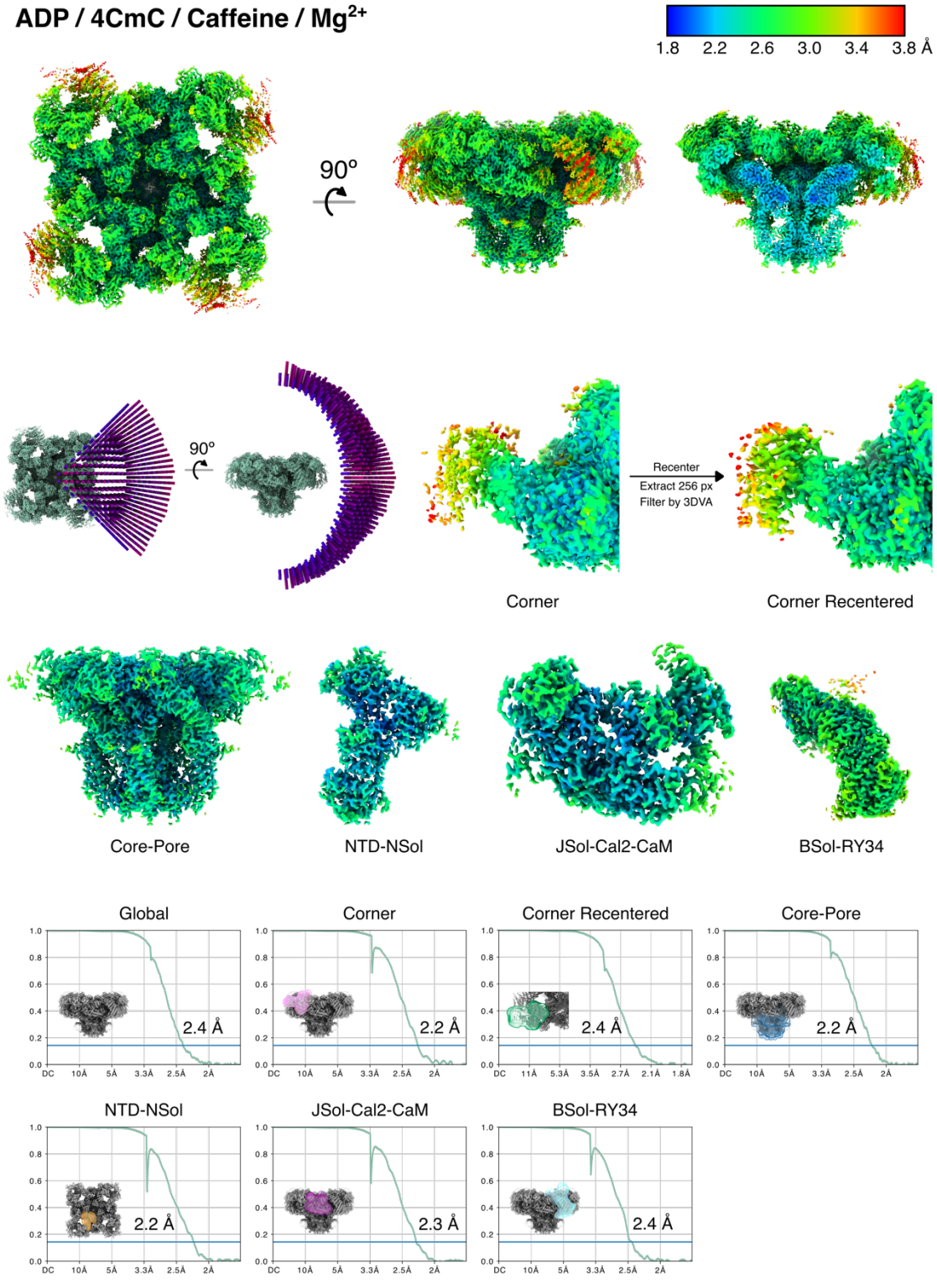

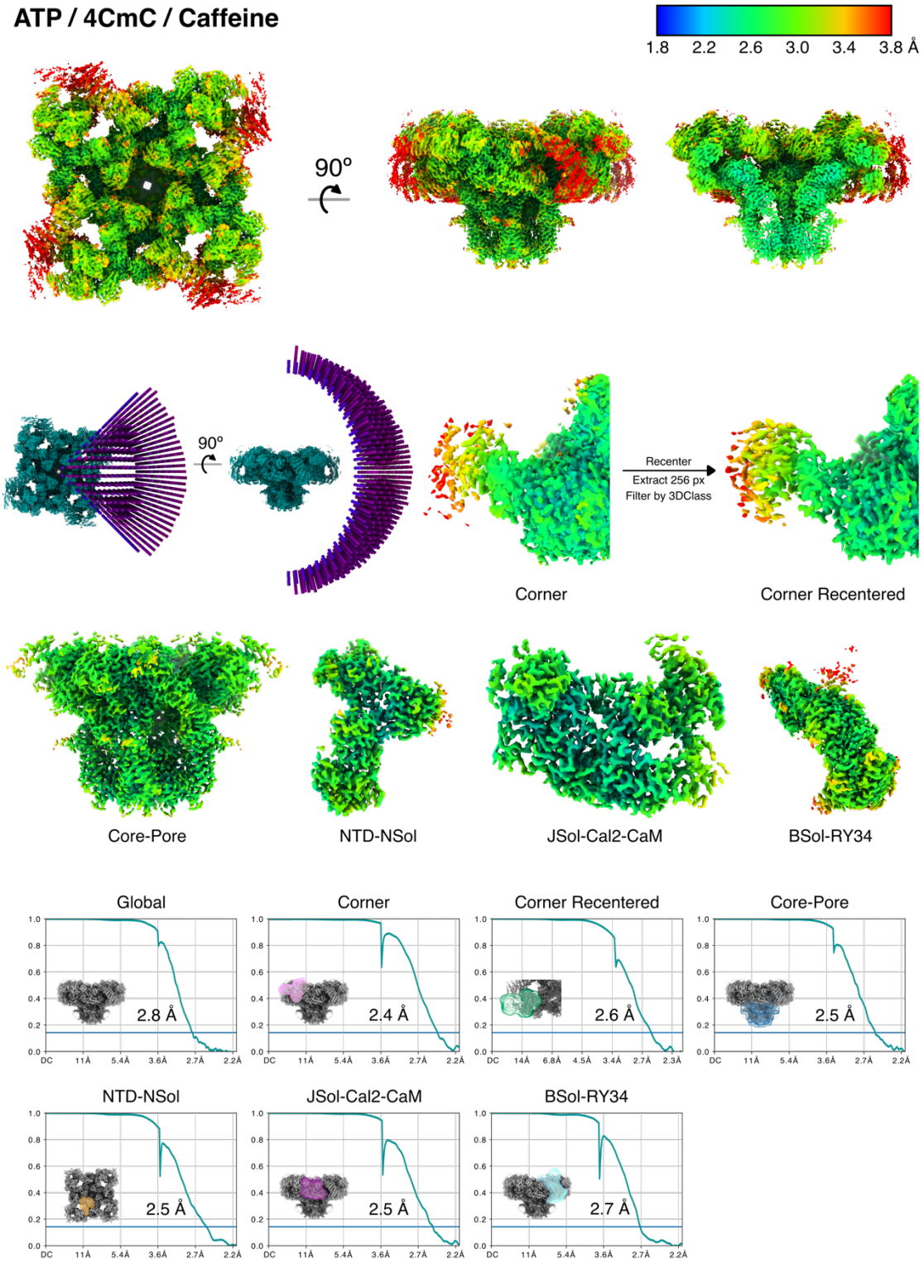

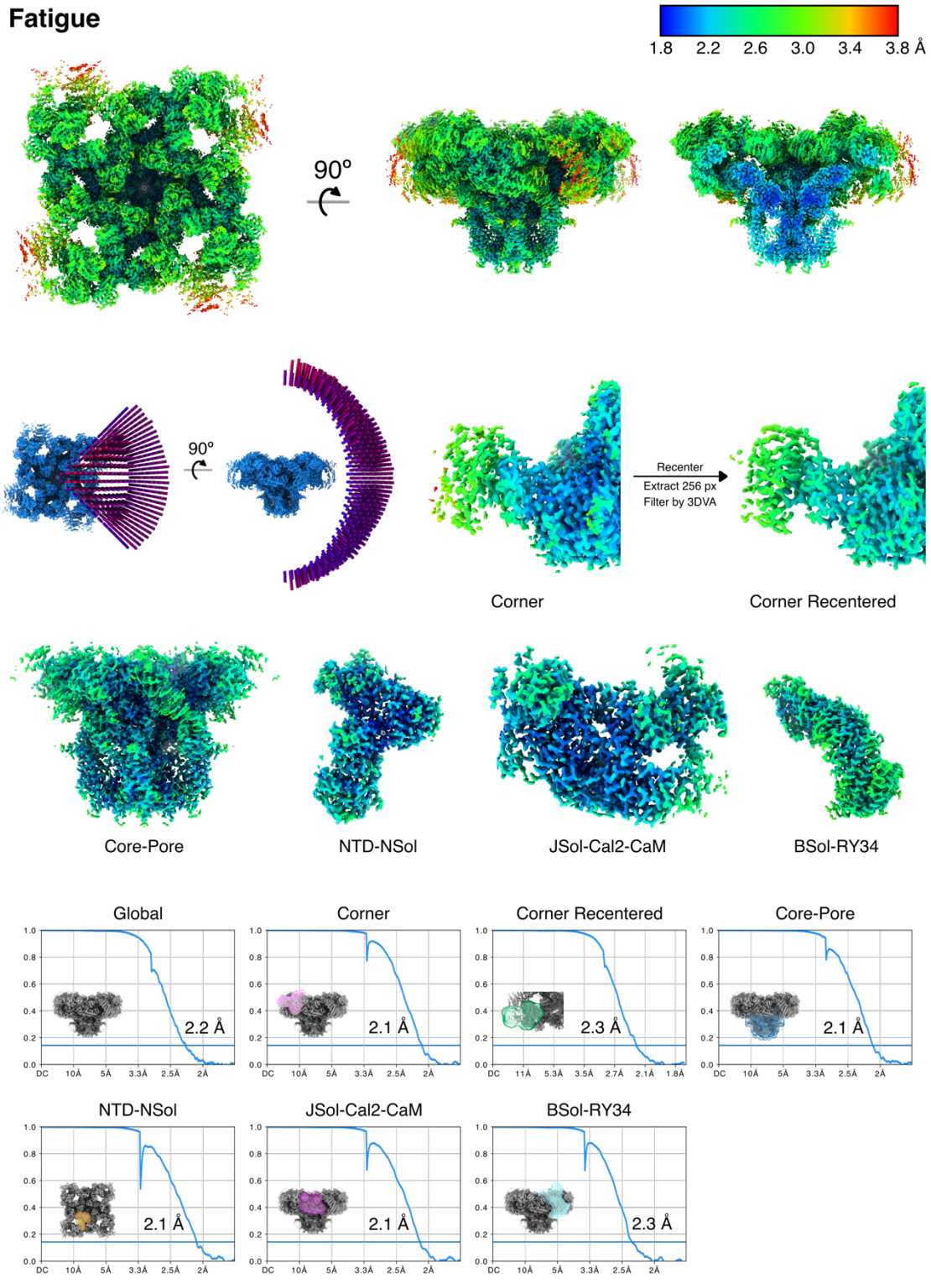

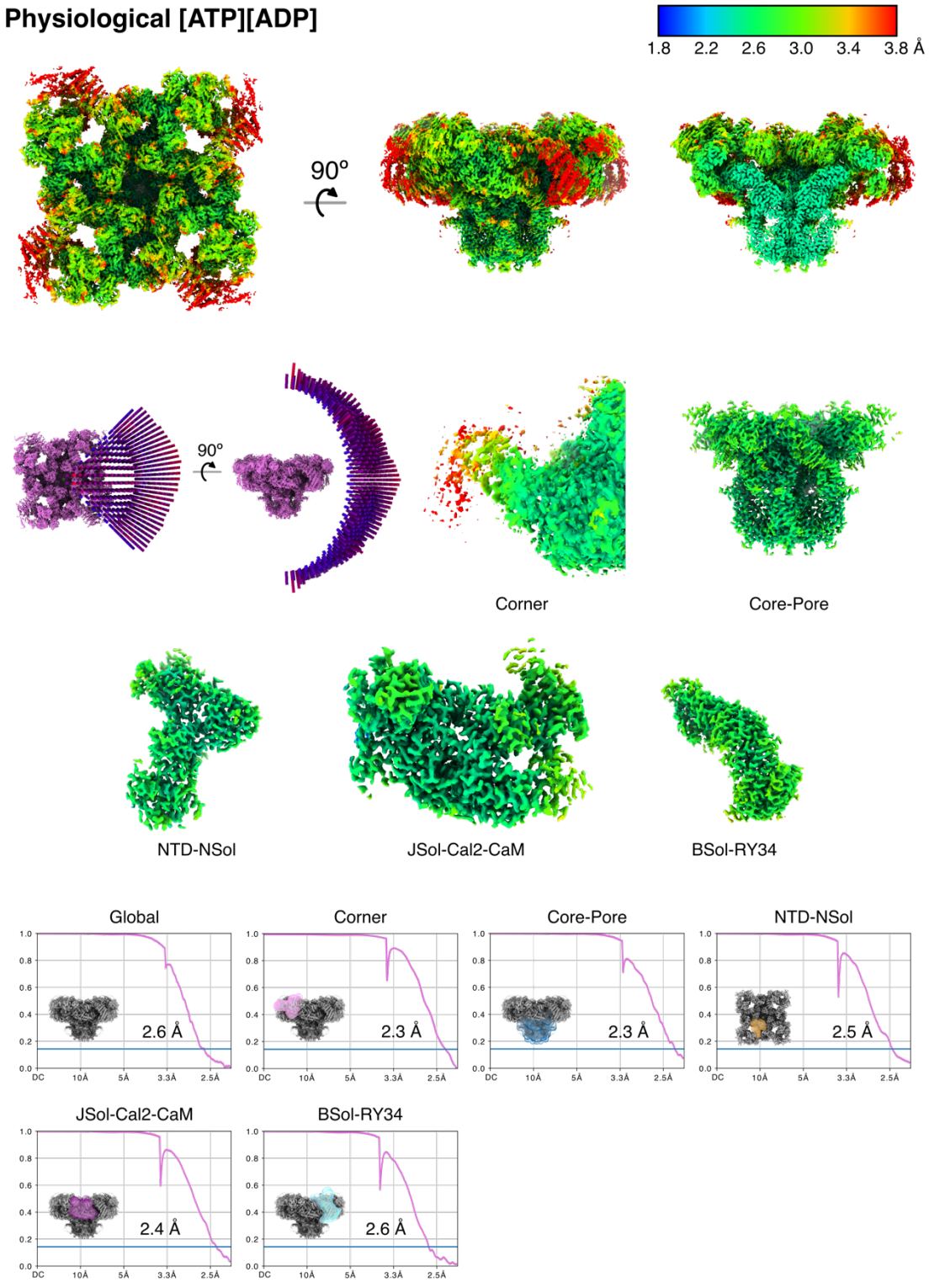

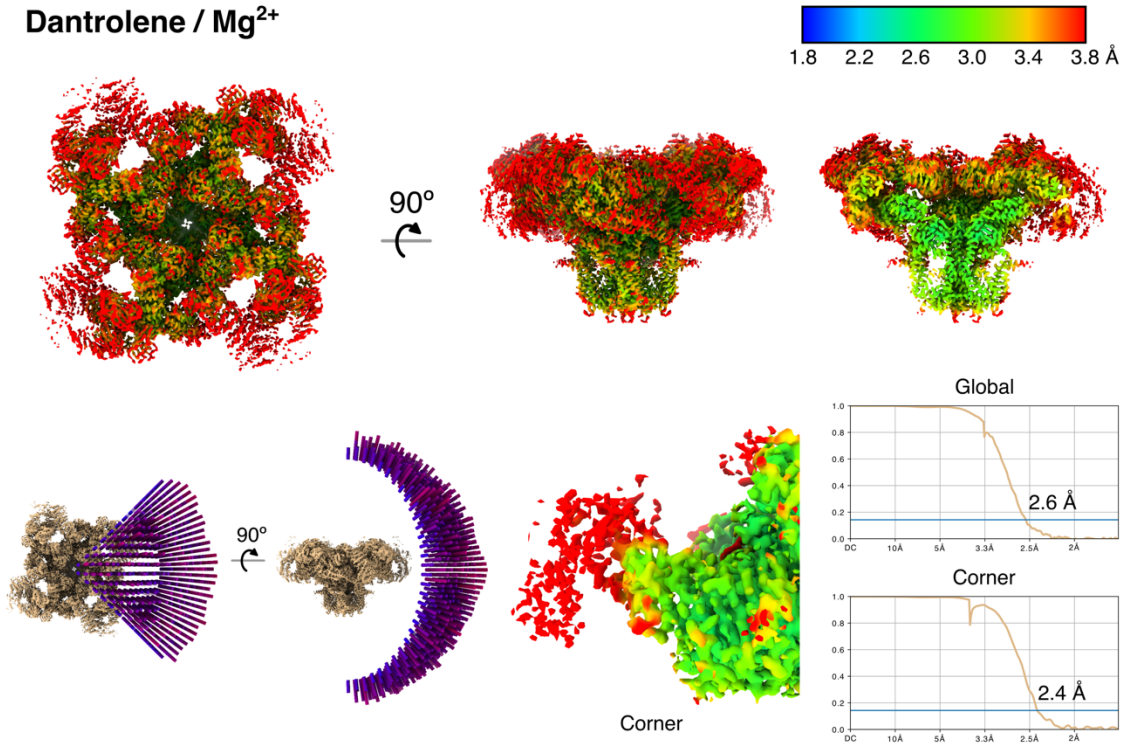

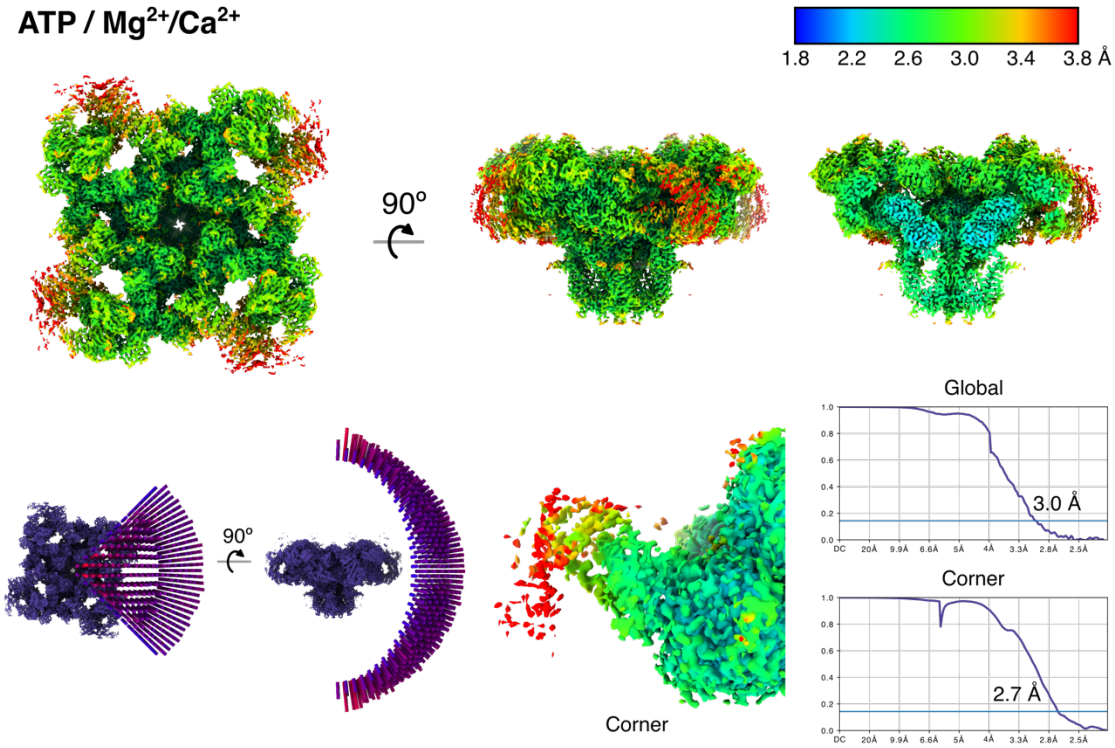

Figure S9: Local resolution and particle orientation plots with FSCs for global and local refinements

Dantrolene / ADP / 4CmC / Caffeine / Mg^{2+}

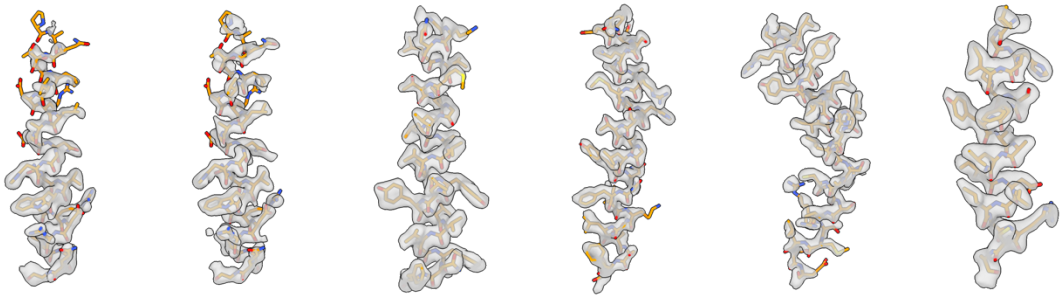

Corner	Corner Recentered	Core Pore	NTD NSol	JSol	BSol
P979 - G1004	P979 - G1004	G4834 - G4858	Q395 - S422	G1705 - E1733	L2418-A2437

Dantrolene / ATP / 4CmC / Caffeine / Mg^{2+}

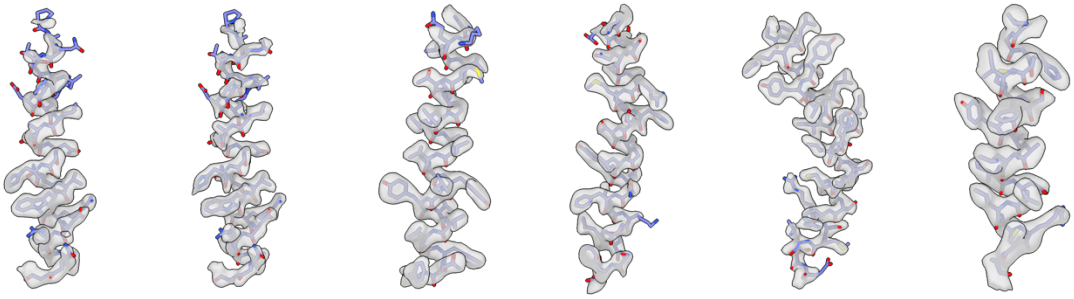

Corner	Corner Recentered	Core Pore	NTD NSol	JSol	BSol
P979 - G1004	P979 - G1004	G4834 - G4858	Q395 - S422	G1705 - E1733	L2418-A2437

ATP / 4CmC / Caffeine

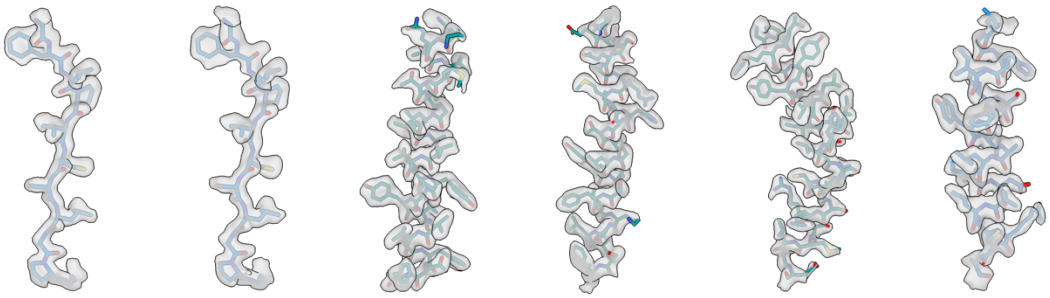

Corner	Corner Recentered	Core Pore	NTD NSol	JSol	BSol
G1187 - G1197	G1187 - G1197	G4834 - G4858	Q395 - S422	G1705 - E1733	L2418-A2437

ADP / 4CmC / Caffeine / Mg^{2+}

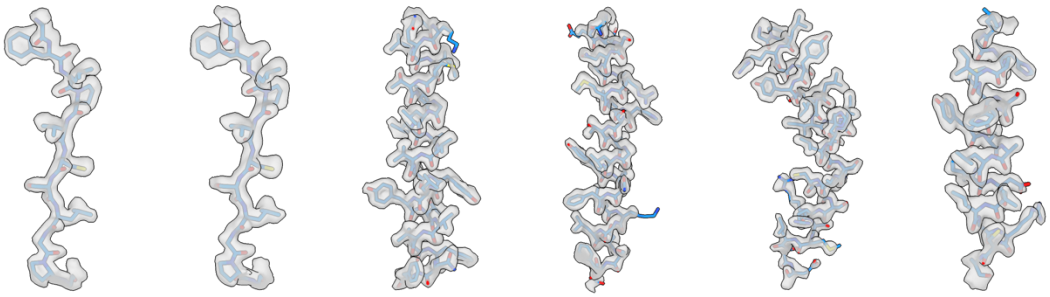

Corner	Corner Recentered	Core Pore	NTD NSol	JSol	BSol
G1187 - G1197	G1187 - G1197	G4834 - G4858	Q395 - S422	G1705 - E1733	L2418-A2437

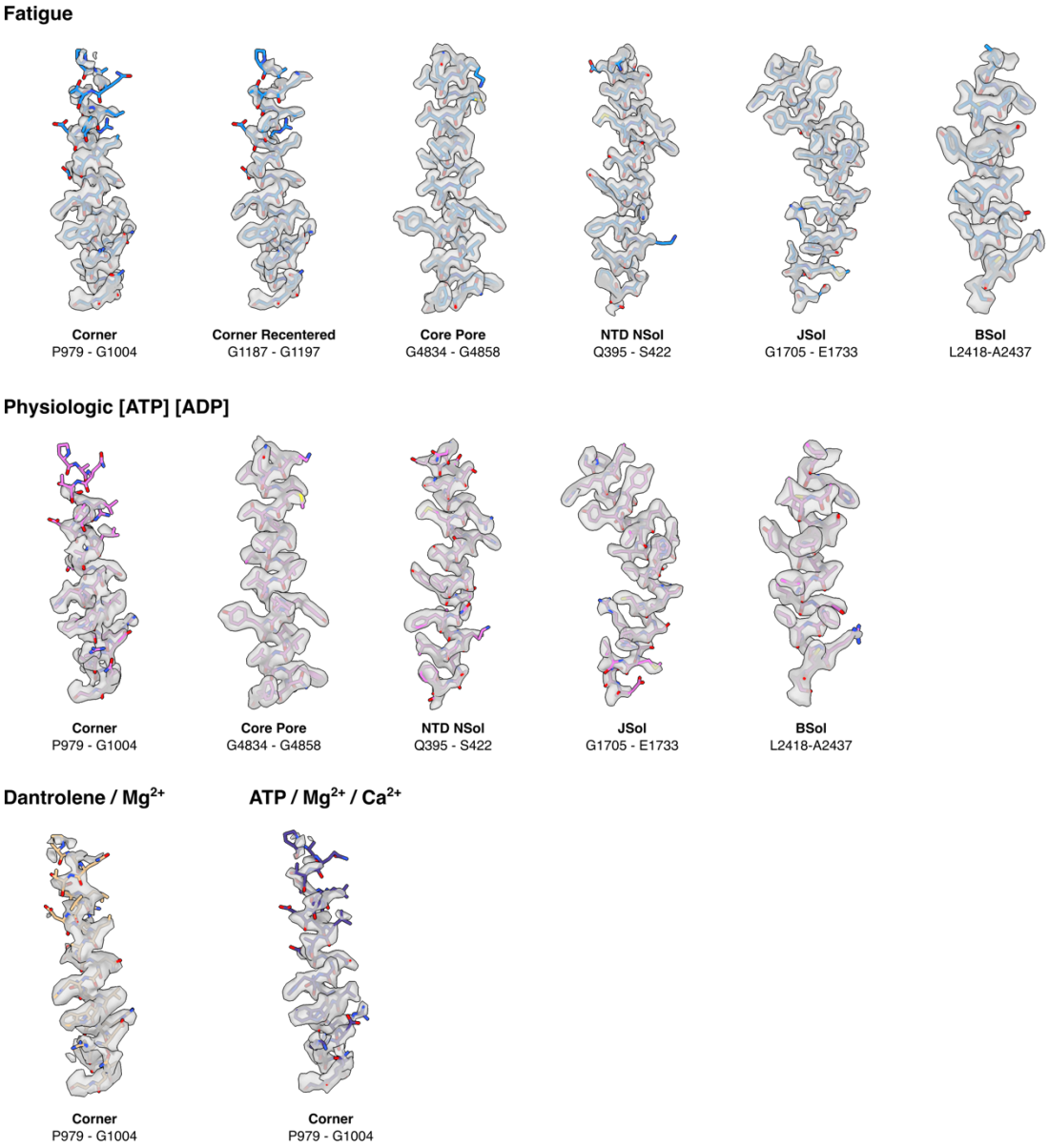

Figure S10: Model/map fit for all local maps of the eight datasets. All maps in the datasets except Dantrolene/Mg^{2+} and ATP/Mg^{2+}/Ca^{2+} were subjected to density modification by *resolve_cryo.em* in *Phenix*.